Dehalogenation and Contemporaneous Removal of Halocarbon using Graphene/Ni Nanoparticles

Maria Sarno, Claudia Cirillo*, Paolo Ciambelli

Department of Industrial Engineering and Centre NANO_MATES, University of Salerno
Via Giovanni Paolo II ,132 - 84084 Fisciano (SA), Italy
clcirillo@unisa.it

Here we report on the chemical reactivity of graphene supported Ni nanoparticles, prepared by an one-step bottom-up chemical strategy in the presence of graphene nanosheets obtained by physical exfoliation of graphite. We have found that graphene/Ni nanoparticles are active for chlordane removal through a two-step mechanism, involving chlordane degradation by Ni nanoparticles supported on graphene and subsequent adsorption of the degraded products by the graphene surface.

1. Introduction

Since its discovery in 2004 (Novoselov et al., 2004), graphene has attracted significant attention in various research fields. In particular, with reference to composite materials, molecular adsorption and reaction on graphene and graphene based composites and their applications in water purification (Sreeprasad et al., 2011; Sreeprasad et al., 2013) have gained momentum recently. Special properties, such as large surface area (Zhu et al.,2010) antibacterial nature (Liu et al., 2011), reduced cytotoxicity (Chang et al.,2011), and tunable chemical properties (Tucek et al., 2014) make these materials very attractive choices for this application. To the best of our knowledge, chemical reactions on graphene and graphene nanocomposites enabling the degradation of halogenated pesticides like chlordane (1,2,4,5,6,7,8,8-octachloro-3a,4,7,7a-tetrahydro-4,7-methanoindane) are unexplored. Chlordane is a versatile, broad-spectrum contact insecticide used mainly for nonagricultural purposes (primarily for the protection of structures, but also on lawn and turf, ornamental trees and drainage ditches). It is also used on corn, potatoes and livestock. When used for termite control, it is applied to the soil by subsurface injection. It has a very low mobility in soil, and it may be a low-level source of contamination in groundwater when applied by subsurface injection. Chlordane is very resistant to chemical and biological degradation. Once in water bodies, it is not removed by photodegradation, hydrolysis or biodegradation and has a high bioaccumulation potential. Levels of chlordane in drinking-water and groundwater that are higher than its solubility have been reported (FAO, 1985). In this paper, we report on the chemical reactivity of few layer graphene−nichel nanocomposites (Ni/FLG) in degrading halogenated pesticides, taking chlordane (1,2,4,5,6,7,8,8-octachloro-3a,4,7,7a-tetrahydro-4,7-methanoindane) as model pollutant. Chlordane was chosen owing to its widespread occurrence, toxicity (McConnachie and Zahalsky, 1992) and persistent nature (Singh et al., 2007). Ni nanoparticles and few layer graphene Ni-FLG have been obtained by a novel one-step "bottom-up" synthetic strategy, providing experimental easiness, potential low-cost fabrication and nanoparticles size control (Altavilla et al., 2013). The resulting nanoparticles are coated with organic chains, which increase the wettability and therefore the dispersion on physical exfoliated, FLG, graphite (Guadagno et al., 2015). We have found that chlordane removal involves a two-step mechanism: degradation of chlordane by nickel nanoparticles and subsequent adsorption of the degraded products by the FLG surface.

2. Experimental Section

2.1 Materials

Ethanol (99.8%, Fluka) and hexane (>95%, Sigma-Aldrich) were used as received. Benzyl ether (99%), 1,2-hexadecanediol (97%), oleic acid (90%), oleylamine (70%), nickel (II) acetylacetonate (90%), were purchased from Aldrich. Graphite powder (microcrystalline, -300 mesh) was purchased from AlfaAesar.

Few layer graphene (FLG) was obtained by graphite sonication in N-methylpyrrolidone (NMP, spectrophotometric grade> 99.0%) (cylindrical vial, 10-25 ml solvent) at a concentration of 10 mg/ml for 1 h at the maximum power of ultrasound (Guadagno et al., 2015; Sarno et al., 2014a; Sarno et al., 2013a; Sarno et al., 2013b).

1000 mg/L of chlordane stock solution was prepared by dissolving the required quantity of chlordane in pure N-hexane (99.9%) and kept under refrigerated condition.

2.2 Preparation of graphene/Ni nanoparticles

The synthesis was carried out using standard airless procedures and commercially available reagents. 0.75 g of Nickel (II) acetylacetonate [$(C_5H_8O_2)_2Ni$], 0.25 g of FLG, 10 mmol of 1,2-hexadecanediol, 6 mmol of oleic acid, 6 mmol of oleylamine, and 20 mL of benzyl ether were magnetically stirred under nitrogen flow.

The mixture was heated to 200°C for 2 h under nitrogen flow and then, under a blanket of nitrogen, heated to reflux (~ 300°C) for 1 h. The black-coloured mixture was cooled to room temperature by removing the heat source. Under ambient conditions, ethanol (40 mL) was added to the mixture, and a black material was precipitated and separated via centrifugation. The obtained product was dissolved in hexane. Centrifugation (10000 rpm, 10 min) was applied to remove any undispersed residue. The product, in the following Ni-FLG, was then precipitated with ethanol, centrifuged (10000 rpm, 10 min) to remove the solvent, and redispersed into hexane.

2.3 Degradation and Adsorption Experiments

All adsorption studies were done in 20 mL batch reactors at room temperature keeping 5 mL of Ni-FLG nanoparticles dispersion (0.01 wt.%) as working volume. A required amount of chlordane stock solution was spiked to the Ni-FLG dispersion to get the working concentration of chlordane at 2 mg/L. The solutions were stirred during 15 min. The liquid was separated from the dispersion using a 200 nm membrane filter paper.

The filtrate, extracted with hexane, was analyzed for residual chlordane and its degradation products using gas chromatography (GC) (ThermoFisher). The analysis conditions were set as follows: run time, 16.5 min; injector temperature, 200 °C; 80°C for 1min+from 80°C to 185°C 10°C/min+185°C for 5 min, 1 mL/min.

2.4 Characterization

Transmission electron microscopy (TEM) images were acquired using a FEI Tecnai electron microscope operated at 200 KV with a LaB_6 filament as the source of electrons, equipped with an EDX probe.

Raman spectra were obtained at room temperature with a micro-Raman spectrometer Renishaw inVia with a 514 nm excitation wavelength (laser power 30 mW) in the range 100-3000 cm^{-1}. XRD measurements were performed with a Bruker D8 X-ray diffractometer using CuKα radiation. Thermogravimetric analysis (TG-DTG) at 10 K/min heating rate in flowing air was performed with a SDTQ 600 Analyzer (TA Instruments) coupled with a mass spectrometer. The KBr technique was applied for determining the FT-IR spectra of the samples by using Vertex 70 apparatus (Bruker Corporation). Spectra were recorded in the scanning range from 4000 to 400 cm^{-1}.

3. Results and discussion

3.1 Ni-FLG Characterization

The XRD pattern of Ni-FLG is shown in Figure 1. The diffraction peaks at 2θ values 39.69°, 41.81°,45.11°, 59.02°, 72.04°, 78.67°, 85.54°, 86.92°, 89.19° are assigned to the Ni nanoparticles (n. 99-101-3040, COD reference database). The (002) reflection from FLG at about 26.7° is clearly visible. FLG flakes have a lateral size of few micrometres. Most of the FLG sample consists of flakes with less than 6 sheets and a number fraction of monolayer graphene (number of monolayers/total number of flakes observed) in NMP dispersions of 22%. In the sample a fraction of flakes (about 6% total based) with a number of sheets between 30 and 40, is also present (Sarno et al., 2014a).
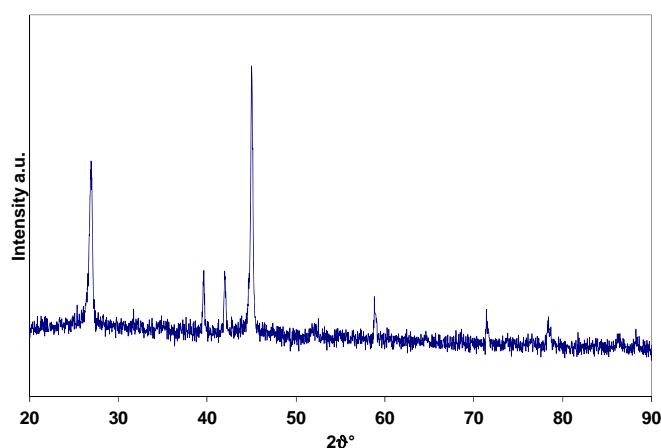
Figure 1. X-ray diffraction pattern of Ni-FLG.

Figure 2 shows a typical Raman spectrum of Ni-FLG excited by 514 nm line in air. In the high wavelength range the typical spectrum of FLG is reported (Guadagno et al., 2015). The two most intense features are the G peak at ~1570 cm^{-1} and the 2D band at ~2700 cm^{-1}, which differs from that typical of graphite, consisting of two components $2D_1$ and $2D_2$, the second with higher intensity than the first. A D-band can be also seen, likely due to the FLG edges (taking into account the laser spot dimension and the flakes size (Sarno et al., 2014a). The band at 518 cm^{-1} is likely due to NiO (Dharmaraj et al., 2006) generated under laser excitation.
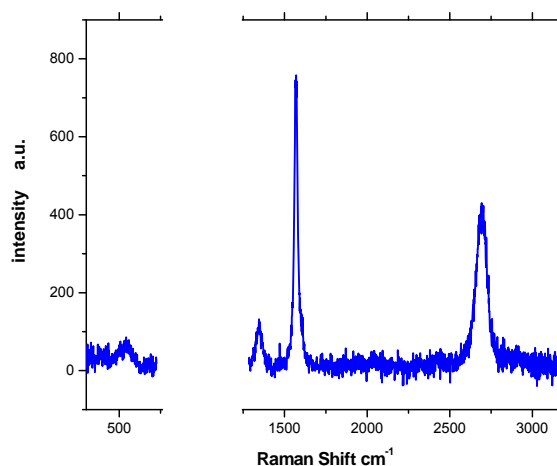
Figure 2. Raman Spectrum of Ni-FLG.

Figure 3 shows bright-field TEM images of Ni-FLG at different magnifications. A lot of particles, 400-500 nm in size and uniformly dispersed on FLG, are visible. In particular, at increasing magnification (the figure inserts),it is seen that the large particles are constituted of nanoparticles with a diameter of 40-50 nm.

The thermal conversion of Ni-FLG in air flow occurred in a single main weight loss step (Figure 4). After solvent release before 100°C, the oxidation of Ni-FLG composite starts (onset temperature 220°C) with the degradation/oxidation of oleylamine/oleic acid organic nanoparticles capping, followed by the oxidation of the FLG (DTG peak at about 695°C). The residue is due to oxidized Ni nanoparticles.
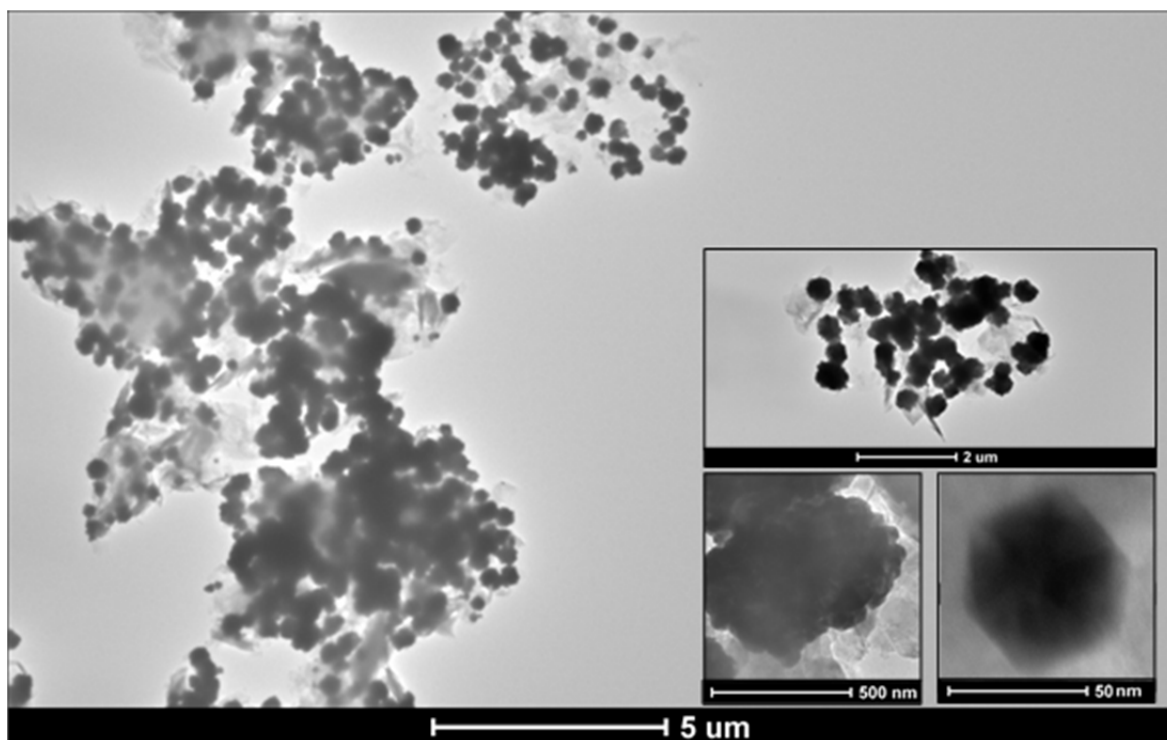
Figure 3. Ni-FLG TEM images, the inserts show the sample at increasing magnification.
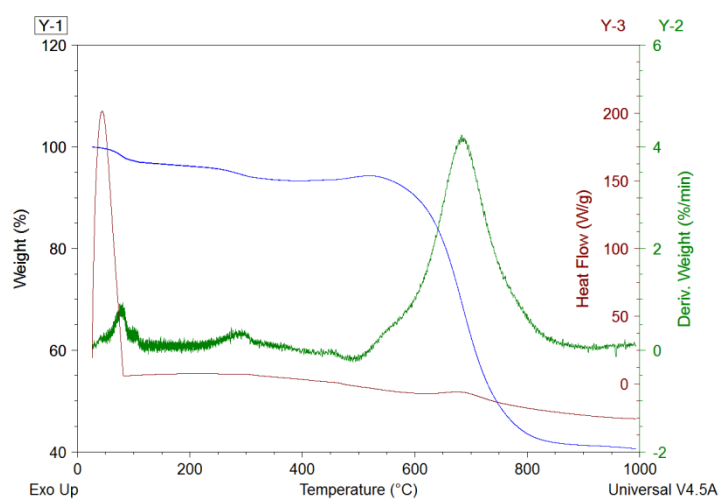
Figure 4. TG-DTG profiles of Ni-FLG.

3.2 Degradation and adsorption tests

To test the composite reactivity, Ni-FLG was taken and chlordane (from the stock solution) was spiked, such that the final concentration of chlordane was 2 mg/L. GC analysis was carried out to monitor the change of chlordane concentration (see the as recorded GC-MS spectrum of chlordane in Figure 5). Initially, chlordane showed a peak around a retention time of 8 minutes and the solvent peak (hexane) appeared during the first two minutes in the GC spectrum.
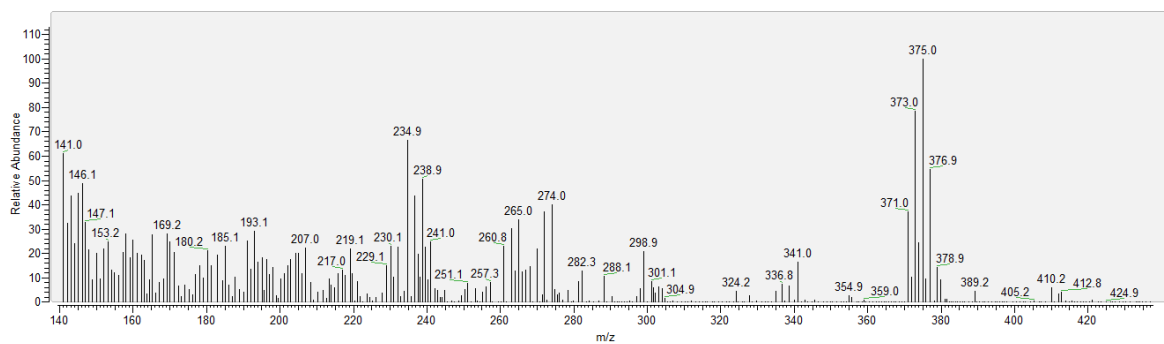
Figure 5. GC-MS spectrum of chlordane.

With increasing the reaction time the chlordane peak started to disappear, implying its removal from the solution, and new peaks, coming from degradation products, became more and more visible at retention time of 4 minutes. Moreover, when the solution was stirred for 15 min, the peaks of both chlordane and reaction products disappeared because of the degradation of the former and the removal of the latter by the Ni-FLG composite, respectively. The chlordane was completely removed in 15 min.
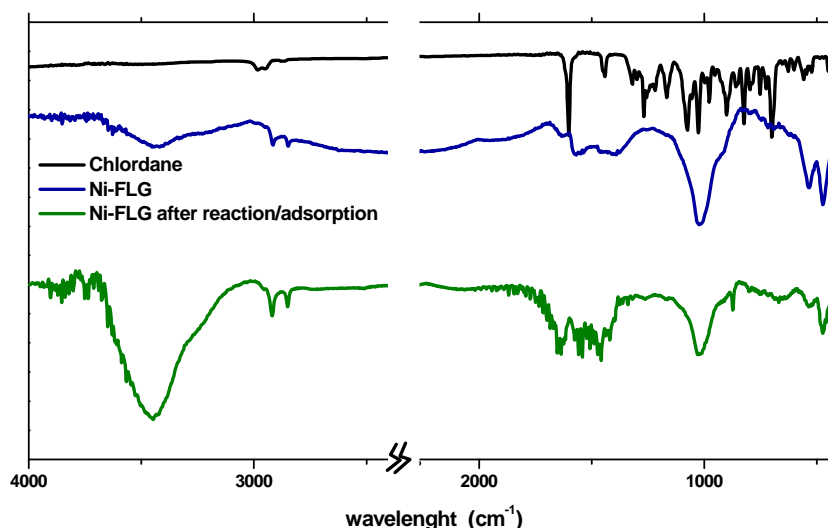
Figure 6. FT-IR spectra of Chlordane, as prepared Ni-FLG and Ni-FLG after 15 min reaction time and filtration.

The FTIR spectrum of chlordane in Figure 6 (black trace) shows the typical peak at 700 cm^{-1} due to C-Cl stretching. In the case of Ni-FLG typical peaks at 1541 and 1649 cm^{-1}, characteristic of the asymmetric νas(COO-) and the symmetric νs(COO-) stretch, due to the bonding of the oleic acid carboxylic groups on the surface of the nanoparticles, are observed. Moreover, the presence of oleylamine as capping agent on the nanoparticles surface is confirmed by the peak characteristics of the oleic group in the 2750-3000 cm^{-1} region, the ν (C=C) stretch mode at 1647 cm^{-1}, and the peak at 1468 cm^{-1} due to the (C-H) bending mode. The IR spectrum of Ni-FLG after reaction/adsorption is also reported in Figure 6 (green trace). New peaks at 887, 1067 and 1139 cm^{-1} are due to the bending vibrations of the =C-H group and the weak peak at 3189 cm^{-1} is due to aromatic C-H stretching. The results give an indication of the formation of aromatic products adsorbed on the Ni-FLG surface. On the other hand, the typical FTIR spectrum of hexane (not shown here) was recorded on the reaction batch after filtration, giving a further confirmation of the adsorption efficiency. The peak around 2800−3000 cm^{-1} is due to the stretching vibration of O-H present in water.

After the reaction with chlordane, Ni-FLG can be separated under the action of a magnetic field.

4. Conclusion

Ni-FLG nanocomposite was prepared by an one-step bottom-up chemical strategy in the presence of graphene nanosheets obtained by physical exfoliation of graphite. TEM images of Ni-FLG at different magnifications show that the nanoparticles have diameter of 40-50 nm and they are organized in aggregates of 400-500 nm in size uniformly dispersed on FLG. A sustainable and efficient way for dehalogenation of halocarbon using Ni-FLG was presented. This process removes completely a persistent organochlorine pesticide in 15 min. The material is very efficient and may be employed for the degradation of other toxic halocarbons.

References

Altavilla C., Sarno M., Ciambelli P., Senatore A., Petrone V., 2013, New 'chimie douce' approach to the synthesis of hybrid nanosheets of MoS_2 on CNT and their anti-friction and anti-wear properties, Nanotechnology 24, 125601 (11pp).

Chang, Y.; Yang, S.-T.; Liu, J. H.; Dong, E.; Wang, Y.; Cao, A.; Liu, Y.; Wang, H., 2011, In vitro toxicity evaluation of graphene oxide on A549 cells. Toxicol. Lett., 200, 201−210.

Dharmaraj N., Prabu P., Nagarajan S., Kim C.H., Park J.H., Kim H.Y., 2006, Synthesis of nickel oxide nanoparticles using nickel acetate and poly(vinyl acetate) precursor Materials, Science and Engineering B 128 111-114.

FAO (1985) Pesticide residues in food - 1984 evaluations. Rome, Food and Agriculture Organization of the United Nations, Joint FAO/WHO Meeting on Pesticide Residues (FAO Plant Production and Protection Paper 67).

Guadagno L., Sarno M., Vietri U., Raimondo M, Cirillo C., Ciambelli P., Graphene-based structural adhesive to enhance adhesion performance, RSC Advances, 2015, 5, 27874.

Liu, S.; Zeng, T. H.; Hofmann, M.; Burcombe, E.; Wei, J.; Jiang, R.; Kong, J.; Chen, Y., 2011, Antibacterial activity of graphite, graphite oxide, graphene oxide, and reduced graphene oxide: Membrane and oxidative stress. ACS Nano, 5, 6971−6980.

McConnachie P.R., Zahalsky A.C., 1992, Immune Alterations in Humans Exposed to the Termiticide Technical Chlordane, Archives of Environmental Health: An International Journal, 47, 295-301.

Novoselov, K. S.; Geim, A. K.; Morozov, S. V.; Jiang, D.; Zhang, Y.; Dubonos, S. V.; Grigorieva, I. V.; Firsov, A. A., 2004, Electric field effect in atomically thin carbon films. Science, 306, 666−669.

Sarno M., Cirillo C., Garamella A., Ciambelli P., 2014a, Synthesis and characterization of electrocatalytic graphene/MoS_2/Ni nanocomposites, Chemical Engineering Transactions, 41, 217-222 DOI: 10.3303/CET1441037.

Sarno M., Cirillo C., Piscitelli R., Ciambelli P., 2013a, A study of the key parameters, including the crucial role of H_2 for uniform graphene growth on Ni foil, J. Mol. Catal. A: Chem. 366, 303-314.

Sarno M., Garamella A., Cirillo C., Ciambelli P., 2014b, MoS_2/MoO_2/graphene electrocatalyst for HER, Chemical Engineering Transactions, 41, 385-390, DOI: 10.3303/CET1441065.

Sarno M., Tamburrano A., Arurault L., Fontorbes S., Pantani R., Datas L, Ciambelli P., Sarto M.S., 2013b, Electrical conductivity of carbon nanotubes grown inside a mesoporous anodic aluminium oxide membrane, Carbon, 55, 10-22.

Singh K.P., Malik A., Sinha S., 2007, Persistent organochlorine pesticide residues in soil and surface water of northern Indo-Gangetic alluvial plains, Environ Monit Assess, 125:147–155.

Sreeprasad, T. S.; Gupta, S. S.; Maliyekkal, S. M.; Pradeep, T., 2013, Immobilized graphene-based composite from asphalt: Facile synthesis and application in water purification. J. Hazard. Mater., 246−247, 213−220.

Sreeprasad, T. S.; Maliyekkal, S. M.; Lisha, K. P.; Pradeep, T., 2011, Reduced graphene oxide−metal/metal oxide composites: Facile synthesis and application in water purification. J. Hazard. Mater., 186, 921−931.

Tucek, J.; Kemp, K. C.; Kim, K. S.; Zboril, R., 2014, Iron-oxidesupported nanocarbon in lithium-ion batteries, medical, catalytic, and environmental applications. ACS Nano, 8, 7571-7612.

Zhu, Y.; Murali, S.; Cai, W.; Li, X.; Suk, J. W.; Potts, J. R.; Ruoff, R. S., 2010, Graphene and graphene oxide: Synthesis, properties, and applications. Advance Materials, 22, 3906−3924.